AGU ADVANCING EARTH AND SPACE SCIENCE

Geophysical Research Letters®

RESEARCH LETTER
10.1029/2021GL097269

Wetting Dynamics of Spontaneous Imbibition in Porous Media: From Pore Scale to Darcy Scale

Chao-Zhong Qin[1,2], Xin Wang[2], Mahmoud Hefny[3,4], Jianlin Zhao[5], Sidian Chen[6], and Bo Guo[6]

[1]State Key Laboratory of Coal Mine Disaster Dynamics and Control, Chongqing University, Chongqing, China, [2]School of Resources and Safety Engineering, Chongqing University, Chongqing, China, [3]Geothermal Energy and Geofluids, Institute of Geophysics, ETH Zürich, Zürich, Switzerland, [4]Department of Geology, South Valley University, Qena, Egypt, [5]Department of Mechanical and Process Engineering, ETH Zürich, Zürich, Switzerland, [6]Department of Hydrology and Atmospheric Sciences, University of Arizona, Tucson, AZ, USA

Key Points:

- We conduct image-based pore-network modeling of spontaneous imbibition in sintered glass beads and Estaillades carbonate
- We illustrate the influence of pore-scale heterogeneity on wetting dynamics and nonwetting entrapment
- We develop a new relative permeability model that incorporates wetting dynamics

Supporting Information:

Supporting Information may be found in the online version of this article.

Correspondence to:

C.-Z. Qin,
chaozhong.qin@gmail.com

Citation:

Qin, C.-Z., Wang, X., Hefny, M., Zhao, J., Chen, S., & Guo, B. (2022). Wetting dynamics of spontaneous imbibition in porous media: From pore scale to Darcy scale. *Geophysical Research Letters*, *49*, e2021GL097269. https://doi.org/10.1029/2021GL097269

Received 29 NOV 2021
Accepted 7 FEB 2022

Author Contributions:

Conceptualization: Chao-Zhong Qin
Formal analysis: Xin Wang
Funding acquisition: Chao-Zhong Qin
Investigation: Chao-Zhong Qin, Xin Wang
Methodology: Chao-Zhong Qin
Project Administration: Chao-Zhong Qin
Resources: Mahmoud Hefny, Sidian Chen
Software: Chao-Zhong Qin, Xin Wang, Jianlin Zhao, Sidian Chen, Bo Guo
Supervision: Chao-Zhong Qin
Validation: Jianlin Zhao, Sidian Chen
Visualization: Xin Wang
Writing – original draft: Chao-Zhong Qin
Writing – review & editing: Chao-Zhong Qin, Mahmoud Hefny, Bo Guo

Abstract

Spontaneous imbibition plays an important role in many subsurface and industrial applications. Unveiling pore-scale wetting dynamics, and particularly its upscaling to the Darcy model, are still unresolved. We conduct image-based pore-network modeling of cocurrent spontaneous imbibition and the corresponding quasi-static imbibition in homogeneous sintered glass beads and heterogeneous Estaillades carbonate. We find that pore-scale heterogeneity significantly influences entrapment of the nonwetting fluid, which in Estaillades is mainly because of the poor connectivity of pores. We show that wetting dynamics significantly deviates capillary pressure and relative permeability away from their quasi-static counterparts. Moreover, we propose a nonequilibrium model for wetting permeability that well incorporates flow dynamics. We implement the nonequilibrium model into two-phase Darcy modeling of a 10 cm long medium. Sharp wetting fronts are numerically predicted, which are in good agreement with experimental observations. Our studies provide insights into developing a two-phase imbibition model with measurable material properties.

Plain Language Summary

The flow of a fluid into a porous matrix by capillary force is encountered in many everyday processes, such as water-flow to reach the tips of trees and water-flow through soils. These processes are examples of spontaneous imbibition. Spontaneous imbibition is also crucial to many industrial applications, ranging from oil recovery and geological sequestration of carbon dioxide to inkjet printing, diapers, and paper sensors. Mostly, the imbibition rate, broadening of the wetting front, and entrapment of the nonwetting fluid are of great interest. In this work, we conduct extensive pore-scale modeling of spontaneous flow in porous media. We illustrate how pore-scale heterogeneity influences imbibition dynamics and entrapment of the nonwetting fluid. To bridge the gap between pore-scale flow dynamics and the Darcy-scale theory of spontaneous imbibition, we develop a nonequilibrium model for wetting permeability that can provide better modeling of spontaneous imbibition at the Darcy scale. Our studies have immediate implications for the applications of oil production from fractured reservoirs, capillary trapping of carbon dioxide, and remediation of nonaqueous liquids in soils.

1. Introduction

In porous media research, spontaneous imbibition is capillary-driven invasion of the wetting phase displacing the nonwetting phase, which is governed by the interplay of capillary force and viscous force. As a typical two-phase flow process, it plays an important role in numerous practical problems such as oil production from fractured reservoirs (Mattax & Kyte, 1962; Morrow & Mason, 2001), remediation of nonaqueous phase liquids in soils (Singh & Niven, 2014), residual trapping in geological carbon dioxide storage (Scanziani et al., 2020), inkjet printing (Wijshoff, 2018), and paper sensors (Rath et al., 2018). Furthermore, spontaneous imbibition has been used to infer wettability of many geological materials (Peng & Xiao, 2017). There have been many fundamental studies of spontaneous imbibition mainly focusing on the prediction of imbibition rates (Akin et al., 2000; Hall & Pugsley, 2020; Kuijpers et al., 2017; Standnes & Andersen, 2017), entrapment of nonwetting fluid (Meng et al., 2015), broadening/roughening of wetting front (Bakhshian, Murakami, et al., 2020; Gruener et al., 2012; Sadjadi & Rieger, 2013; Soriano et al., 2005; Zahasky & Benson, 2019), and Darcy-scale capillary pressure and relative permeability (Alyafei & Blunt, 2018; Haugen et al., 2014; Mason & Morrow, 2013).

According to how the wetting fluid enters and exits a medium, spontaneous imbibition can be categorized into cocurrent spontaneous imbibition and countercurrent spontaneous imbibition. In cocurrent spontaneous imbibition, the wetting phase enters a porous medium through one boundary, while the nonwetting phase is displaced from the medium via other boundaries. By contrast, in countercurrent spontaneous imbibition, the wetting and nonwetting phases respectively enter and leave a porous medium via the same boundary. In practice, they may coexist and switch from one to the other depending on the viscosity ratio and the domain size (Haugen et al., 2014). Overall, the two imbibition processes are distinct in pore-filling mechanisms, imbibition dynamics, and Darcy-scale material properties. For countercurrent spontaneous imbibition (e.g., the scenario of "*one end open*"), experiments show that the imbibition rate commonly is linearly proportional to the square root of imbibition time, and many scaling groups have been developed (K. S. Schmid & Geiger, 2012; Mason & Morrow, 2013). However, it is still unclear how capillary backup pressure and backup saturation evolve in time, which are important input parameters to the Darcy-scale modeling. Countercurrent spontaneous imbibition may be close to quasi-static; nevertheless, the difference between the two is still unclear. Therefore, it is not confident to use conventionally measured capillary pressure and relative permeability curves in the Darcy-scale modeling.

There is a long history of research on cocurrent imbibition, which was pioneered by Lucas and Washburn's work on imbibition in a capillary tube (Washburn, 1921). By treating a porous medium as a bundle of capillary tubes, various analytical/semi-analytical models have been developed to predict the imbibition rate (Cai et al., 2021; Standnes, 2010). Likewise, by assuming a sharp wetting front and neglecting the nonwetting-phase resistance and gravity, the wetting penetration depth can be simply given by the single-phase Darcy model as $L = \sqrt{2\mathrm{kp}^c/\varepsilon\mu}\sqrt{t}$, where ε is the porosity, μ is the dynamic viscosity, k is the wetting permeability depending on the entrapment of the nonwetting phase, p^c is the Darcy-scale capillary pressure, and t is the imbibition time. To quantitatively predict the imbibition rate, one needs to know wetting permeability and capillary pressure in advance. However, it is still unclear how to relate them to conventional material properties of a porous medium such as pore-size distribution, wettability, quasi-static capillary pressure curve, and relative permeability measured under steady state (Akbarabadi & Piri, 2013; Gao et al., 2020; Krause & Benson, 2015; Ruprecht et al., 2014). Moreover, in the case of late stage of imbibition or imbibition with low viscosity ratios (e.g., water imbibes into an oil-saturated medium), the assumption of sharp wetting front will no longer valid, necessitating the use the two-phase Darcy model (Zarandi & Pillai, 2018).

Many studies of the Darcy-scale modeling of cocurrent spontaneous imbibition have been conducted, primarily for the air-water system where water is the wetting phase. It is acknowledged that dynamics of self-determined spontaneous imbibition causes Darcy-scale capillary pressure and relative permeability to deviate from their values at equilibrium. Therefore, in most studies, assumed or experimentally fitted relationships that differed from those measured under steady-state/quasi-static conditions were usually used (Alyafei et al., 2016; K. S. Schmid et al., 2016; Suo et al., 2019; Zahasky & Benson, 2019). It is unclear how they are related to the quasi-static counterparts and also pore-scale events. Furthermore, those fitted relationships may be not applicable to imbibition away from the inlet or cannot be extended to other fluid systems of imbibition. Regarding the effect of dynamics (or nonequilibrium) on capillary pressure and relative permeability, there are a few pioneering studies including the well-known tau term in capillary pressure proposed by Hassanizadeh and Gray (Hassanizadeh & Gray, 1990; Zhuang et al., 2017), and the effective saturation proposed by (Barenblatt et al., 2003). The benefit of those models is that they may physically link the nonequilibrium effect to conventional capillary pressure and relative permeability. However, relevant studies in spontaneous imbibition are scarce, which will be addressed in this work.

There have been other challenges in the prediction of spontaneous imbibition, such as the effects of pore heterogeneity, initial wetting saturation, gravity, and mixed-wettability on the imbibition rate and entrapment of the nonwetting fluid (or residual saturation) (Bartels et al., 2019). In this regard, pore-scale studies will be indispensable. Because pore-scale events in spontaneous imbibition, particularly cocurrent spontaneous imbibition, are so quick that current imaging techniques may not capture them, the pore-scale modeling will be tremendously beneficial. Previous pore-scale modeling of spontaneous imbibition have been limited to synthetic 2-D porous media or a porous domain smaller than the REV size (Bakhshian, Rabbani, et al., 2020; Diao et al., 2021; Liu et al., 2020; Rokhforouz & Akhlaghi Amiri, 2018; Zheng et al., 2021). As a result, the obtained pore-scale information was not upscaled to Darcy-scale capillary pressure and relative permeability. Alternatively, the efficient pore-network modeling is promising (Aghaei & Piri, 2015; Chen et al., 2020; Joekar-Niasar et al., 2010). In this

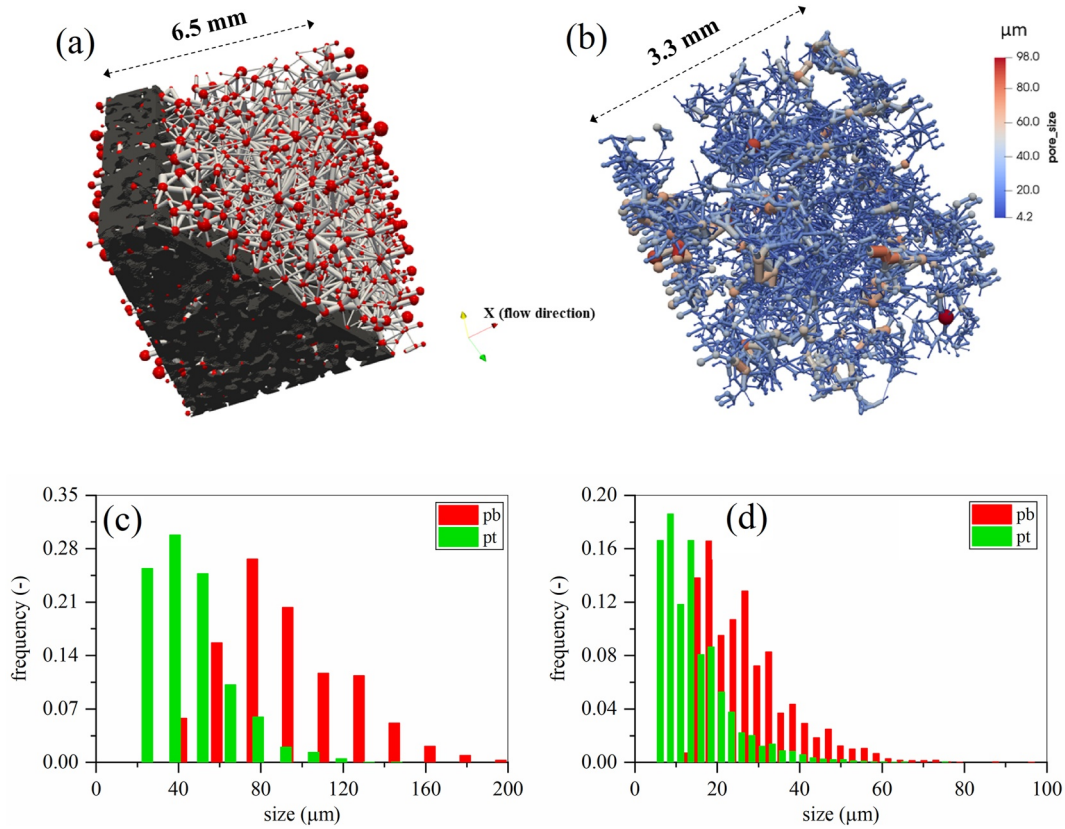

Figure 1. Details of the two pore networks: (a) the extracted pore network and solid phase of the pore medium of sintered glass beads; (b) the extracted pore network of Estaillades, the colormap shows the distribution of inscribed radii; (c) the pore-body inscribed radius and the pore-throat inscribed radius distributions of sintered glass beads, and (d) of Estaillades where the legends of "pb" and "pt" denote pore bodies and pore throats, respectively.

paper, we study cocurrent spontaneous imbibition and quasi-static imbibition in both homogenous and heterogeneous porous media using our in-house pore-network simulator, which has been verified through comparisons to direct numerical simulations (C. Z. Qin & van Brummelen, 2019; C. Qin et al., 2021). Based on the pore-scale findings, we aim to (a) show the effect of pore-scale heterogeneity on imbibition dynamics and nonwetting entrapment, (b) to demonstrate the deviation of capillary pressure and relative permeability curves in spontaneous imbibition from their quasi-static ones, and (c) develop a relative permeability model for the wetting phase in spontaneous imbibition that takes imbibition dynamics into account.

2. Materials and Methods

We use sintered glass beads and Estaillades carbonate (Muljadi et al., 2016) as our porous samples where microporosity in Estaillades is not considered (Gao et al., 2019). PoreSpy is used to extract their pore networks (Gostick, 2017). As shown in Figure 1a, the porous medium of sintered glass beads features homogeneous, which also resembles highly permeable sandstones in terms of complex pore structures. The extracted pore network of Estaillades carbonate, shown in Figure 1b, exhibits significant pore-scale heterogeneity. Isolated pore spaces are determined to account for approximately 14% of total pore volume. The pore-size distributions of the two samples are shown in Figures 1c and 1d. In Estaillades, the majority of pores locate in the left branch of the pore-size distribution.

The details of the pore networks and their material properties are given in Table S1 in Supporting Information S1. We run Lattice-Boltzmann simulations of each pair of watersheds in the pore networks to obtain its conductance, and assign it to the corresponding pore throat (Zhao et al., 2020). A similar practice was also used by (Raeini et al., 2017) in their algorithm of pore-network extraction. The homogenous medium of sintered glass beads

is highly permeable with a permeability of 113.2 D, while the heterogeneous Estaillades has a much smaller permeability of 0.303 D. Half of the Estaillades was used by (Muljadi et al., 2016) to study the heterogeneity on non-Darcy flow behavior, in which a permeability of 0.172 D was reported.

Given a mean pore size (i.e., radius) and permeability, the tortuosity, τ, may be calculated by the empirical model: $k = \varepsilon r^2/8\tau^2$ (Kuijpers et al., 2017). In such way, the tortuosity values of sintered glass beads and Estaillades are 1.8 and 6.9, respectively. Overall, a wide pore-size distribution combined with poor connectivity (see Figure S1 in Supporting Information S1 for the distributions of coordination number) result in strong pore-scale heterogeneity of Estaillades with high tortuosity.

To fulfill our objectives, we concentrate on the early stage of cocurrent spontaneous imbibition and the corresponding quasi-static imbibition. Initially, the media are fully saturated with the nonwetting fluid. We conduct free spontaneous imbibition with one end face in contact with a wetting reservoir and the other end face in contact with a nonwetting reservoir. The four surrounding faces are sealed. Numerically, we depress any countercurrent imbibition at the wetting reservoir. Although the used samples may be mixed-wettability, particularly for Estaillades (Lin et al., 2021), uniform wettability is assumed on purpose. We do not focus on specific fluids, and assume some wettability-alteration technique (Alyafei & Blunt, 2016), which allows us to set up four contact angel values (20°, 40°, 60°, and 80°) for three pairs of fluids with the viscosity ratios of 55.9, 1.0, and 0.1. Here, A viscosity ratio is defined as $M = \mu^w/\mu^n$, where μ^w and μ^n are the wetting and nonwetting dynamic viscosities, respectively. A viscosity ratio of 55.9 is for a water-air system, while the viscosity ratios of 1.0 and 0.1 are used to mimic water-oil systems and/or water-CO_2 systems. In all case studies, water is treated as the wetting fluid, and surface tension of 0.073 N/m is assumed for simplicity. In the analysis of wetting permeability, an advancing contact angle of 40° for water is assumed. Text S1 in Supporting Information S1 describes the dynamic pore-network model in detail. Its source codes and all numerical results are available at Figshare (Qin, 2021).

3. Results and Discussion

3.1. Effect of Pore-Scale Heterogeneity on Spontaneous Imbibition

Spontaneous imbibition of water into dry sintered glass beads and Estaillades has been conducted under four different contact angle values. Figure 2a shows the temporal evolutions of the network-scale water saturation in sintered glass beads. The four imbibition curves are smooth due to the pore-scale homogeneity of sintered glass beads. Figure 2c shows the scaled imbibition rates (i.e., $S/\sqrt{t}$, where S is the network saturation and t is the imbibition time) versus the network saturation, and the reference imbibition rate was obtained under the contact angle value of 40°. It is seen that all imbibition rates more or less lump to a constant except for those at the initial and final stages of imbibition, which indicates the imbibition rate in sintered glass beads is linearly proportional to the square root of imbibition time, and the imbibition rate can be adequately scaled with $\sqrt{\cos\theta}$. Moreover, with respect to the early stage of spontaneous imbibition, the medium size of sintered glass beads approaches its REV size. We observe that residual saturation (i.e., the amount of trapped air) in homogenous sintered glass beads is very low (around 0.06), which is in consistence with experimental data (Kuijpers et al., 2017). Figure 2b shows the temporal evolutions of water saturation in Estaillades. Its pore-scale heterogeneity is clearly reflected in the imbibition curves. A few peaks of the imbibition rate are seen in Figure 2d. The heterogeneity, however, has little influence on the scaling behavior of the imbibition rate, which indicates the dominance of MTM (main terminal meniscus) move in the pore-filling (C. Qin et al., 2021). Compared with sintered glass beads, the REV size of Estaillades should be much larger. Moreover, residual saturation in Estaillades is much higher up to 0.36. This value is in good match with experimental data (one can refer to Figure 4a in Alyafei et al., 2016).

Pore-scale water distributions in sintered glass beads and Estaillades in the end of spontaneous imbibition are shown in Figure S2 in Supporting Information S1. The air-water system was considered with the static contact angle value of 40°. It is seen that a few partially filled/dry pores spread over the medium in sintered glass beads, while a large number of dry pores present in Estaillades in the form of individual clusters. Obviously, the pore-scale heterogeneity of Estaillades results in severe entrapment of air. There is no preference for air to be trapped in small pores for both sintered glass beads and Estaillades, which indicates the cofilling of small and large pores at the early stage of imbibition. Moreover, the entrapment of air in heterogeneous Estaillades is primarily due to the poor connectivity of pores, which may be termed as topological trapping. Movies S1 and S2 in Supporting Information S1 show the dynamic imbibition processes in sintered glass beads and Estaillades, respectively.

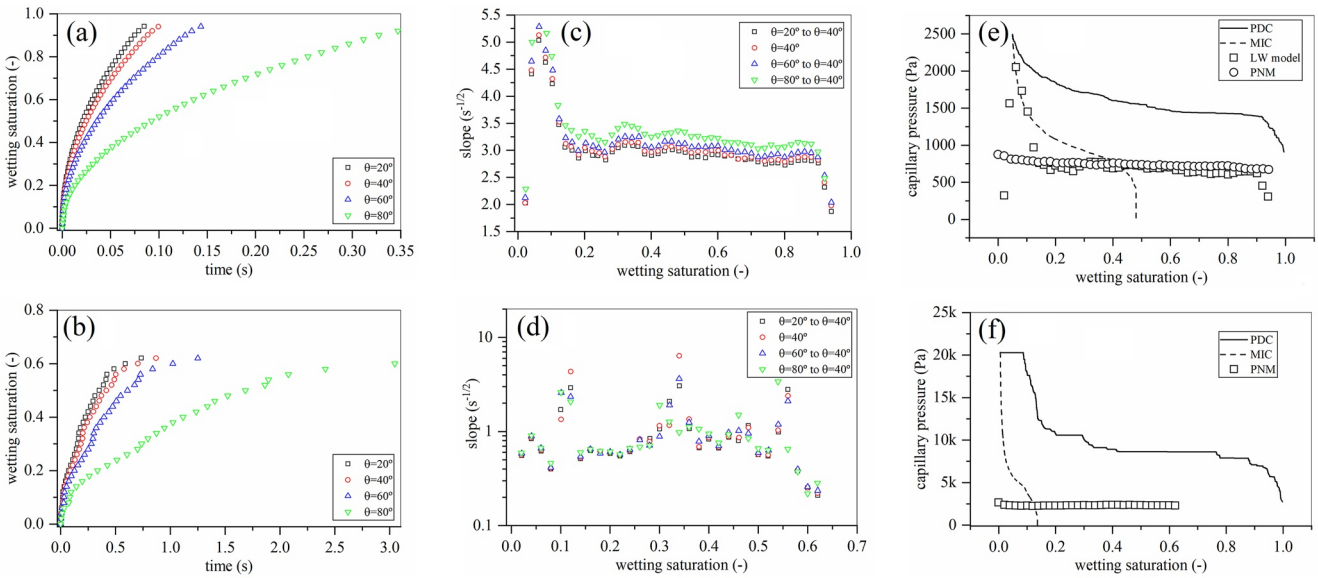

Figure 2. Spontaneous imbibition of water into dry sintered glass beads and Estaillades under different contact angle values. (a) The network water saturation versus the imbibition time for sintered glass beads, and (b) for Estaillades. (c) The scaled imbibition rates with the contact angle value of 40° versus the network saturation for sintered glass beads, and (d) for Estaillades. The scaling is done by multiplying the imbibition rate of interest by $\sqrt{cos40°/cos\theta}$, where θ is the scaled contact angle. (e) The capillary pressure values predicted by the pore-network model (PNM) and the Lucas-Washburn model, the primary drainage curve (PDC), and the main imbibition curve (MIC) for sintered glass beads. (f) The capillary pressure values predicted by the PNM, the PDC, and the MIC for sintered glass beads. The air-water system is considered with the viscosity ratio of 55.9.

A sharp wetting front with a few pores roughening moves through sintered glass beads. Cofilling dynamics is clearly seen. In heterogeneous Estaillades, however, the imbibition follows preferential pathways, leaving air in poorly connected regions. Although heterogeneity has pronounced influence on pore-scale imbibition dynamics, it is worth noting that at the REV scale a sharp wetting front holds in both sintered glass beads and Estaillades for the air-water system (Alyafei et al., 2016). The main differences lie in the REV size, residual saturation, and roughening of wetting front.

There are two ways to obtain average-scale capillary pressure. One way is that we calculate interface-averaged capillary pressure directly from the pore-scale simulation results. The other is that we use the Lucas-Washburn-type model, $S = \sqrt{2k^w p^c/\varepsilon\mu^w d^2}\sqrt{t}$, where d is the medium length. From the pore-scale results, we know the values of $\sqrt{2k^w p^c/\varepsilon\mu d^2}$ which are equal to $S/\sqrt{t}$, and the wetting permeability, k^w, at the end of imbibition. Together with the other known material properties (i.e., ε, μ^w, and d), capillary pressure can be calculated by $S^2\varepsilon\mu^w d^2/2k^w t$. Figures 2e and 2f show the comparisons of capillary pressure values predicted by the dynamic pore-network modeling, the LW model, and the quasi-static drainage and imbibition. As distinct from the dynamic pore-network modeling, the quasi-static modeling neglects viscous forces, and follows the algorithm of invasion-percolation, together with key displacement events such as piston-move, snap-off, and cooperative filling of pore bodies (Patzek, 2001). We show that wetting dynamics in spontaneous imbibition significantly deviates the capillary pressure curve away from its quasi-static counterpart for either sintered glass beads or Estaillades, which would impose a challenge in setting up material properties in the Darcy-scale modeling. For sintered glass beads, the capillary pressure has the value of around 700 Pa, which stays at the end of the quasi-static main imbibition curve (MIC). Moreover, the capillary pressure values predicted by the dynamic pore-network modeling and the LW model match well for homogenous sintered glass beads.

3.2. Relative Permeability of the Wetting Fluid

Two approaches are available to determine relative permeability of a porous medium. The steady-state approach is one in which a moderate range of wetting saturation can be experimentally accomplished in the presence of low capillary number flows (Akbarabadi & Piri, 2013; Gao et al., 2020). In the other approach, relative permeability is numerically solved based on the information of pore-scale phase distributions, which may be obtained by the

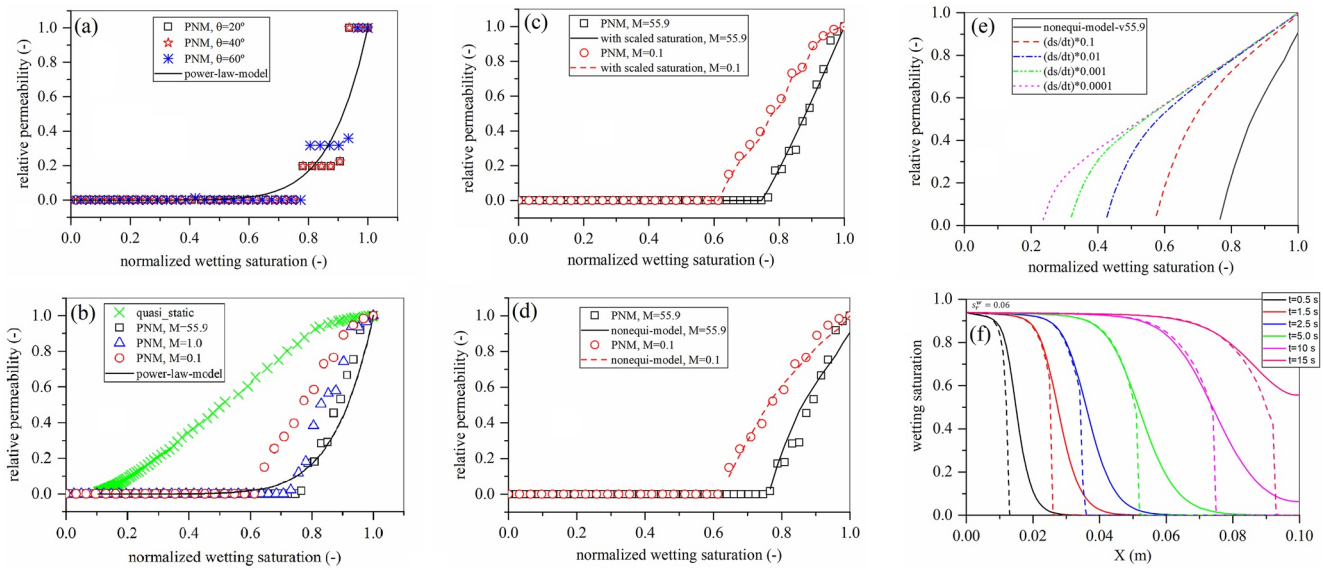

Figure 3. (a) Wetting relative permeability under different contact angle values for Estaillades by the pore-network model (PNM) and the power-law model (the exponent is set to 8). The viscosity ratio is 55.9 for the air-water system. (b) Wetting relative permeability under different viscosity ratios by the PNM, quasi-static, and by the power-law model (the exponent is set to 8) for sintered glass beads under the contact angle value of 40°. (c) The wetting relative permeability for sintered glass beads under high and low viscosity ratios predicted by the PNM and the power-law model with scaled saturation (the exponent is set to 1.1), and (d) predicted by the PNM and the nonequilibrium model (the exponent is set to 1.1). (e) Effect of wetting dynamics on the water relative permeability for sintered glass beads. (f) Temporal water saturation profiles along the 10 cm long sintered glass beads during spontaneous imbibition.

imaging technique (Berg et al., 2016) or the pore-scale modeling (Al-Futaisi & Patzek, 2003). Here, we use the latter approach, and pore-scale phase distributions are from the dynamic and quasi-static pore-network modeling. Figure 3a shows the water relative permeability under different contact angle values for Estaillades. Under the premise of uniform wettability, the water relative permeability is not sensitive to the contact angle. Due to the heterogeneity and the limit of the study domain, smooth relative permeability curves are not obtained. Nevertheless, the power-law model's relative permeability curve with an exponent of 8 locates within those relative permeability values. As shown in Figure 3b, the power-law model with an exponent of 8 can moderately suit the water relative permeability for sintered glass beads in the air-water system. From the pore-scale perspective, we may understand why some Darcy-scale models of spontaneous imbibition entail a large exponent value in their power-law or Corey expressions for the water relative permeability (Alyafei et al., 2016; K. S. Schmid et al., 2016; Suo et al., 2019), in order to produce sharp wetting fronts. The influence of wetting dynamics on water relative permeability is pronounced in Figure 3b. Wetting dynamics deviates the wetting relative permeability away from its quasi-static curve (the relative permeability of primary drainage and main imbibition for sintered glass beads is given in Figure S3 in Supporting Information S1). The deviation is reduced when the viscosity ratio decreases, because flow dynamics are reduced.

We have demonstrated unequivocally that wetting relative permeability significantly depends on wetting dynamics. Now, the challenge lies in how to incorporate dynamics into the wetting relative permeability while still relating the relative permeability to its measured quasi-static/steady-state equivalent. We propose two models, and then testify them against the pore-scale results. First, as usual, we fit the quasi-static relative permeability by the power-law model as $k_r^w = (s^e)^{1.1}$ as shown in Figure S4 in Supporting Information S1 with the normalized saturation, $s^e = s/(1-s_r)$, where s_r is the residual saturation of 0.52. Notice that the wetting permeability is written as $k^w = 0.114k_0(s^e)^{1.1}$, where k_0 is the intrinsic permeability and $0.114k_0$ is the wetting permeability at the residual saturation. A nearly linear relation between the wetting relative permeability and the normalized saturation is predicted for imbibition, which is also seen in steady-state measurements (Akbarabadi & Piri, 2013; Ruprecht et al., 2014). It is worth noting that an estimated wetting relative permeability from the high-wetting-saturation portion of the drainage curve may not be applicable to spontaneous imbibition. When normalizing wetting saturation in spontaneous imbibition with the viscosity ratios of 55.9 and 0.1, the residual saturation values are 0.06 and 0.38, respectively, which are predicted by the pore-network modeling. In Figure 3b, we further observe a critical

saturation value for each case of the viscosity ratio, below which the wetting phase does not form a conducting pathway. In light of this observation, we propose to scale the normalized saturation with respect to the critical saturation so that a final effective saturation is written as $s^{fe} = (s^e - s_c)/(1 - s_c)$. Then, we substitute the normalized saturation with the final effective saturation in the power-law model of quasi-static relative permeability, and set the relative permeability to zero whenever $s^{fe} < 0$. As a result, the wetting relative permeability for sintered glass beads under a high and a low viscosity ratio predicted by the power-law model is shown in Figure 3c, which matches the relative permeability by the pore-network modeling very well. However, the critical saturation value should be predescribed, which obviously depends on wetting dynamics. In order to fulfill the development of this sort of permeability model, we need to further develop a relation between critical saturation and wetting dynamics, which is beyond the scope of this paper.

Alternatively, motivated by the concept of nonequilibrium saturation in (Barenblatt et al., 2003) and the work of dynamic capillarity in (Zhuang et al., 2017), we propose the second model of wetting relative permeability as:

$$k_r^w = \left(s^e - m(s^e)^n \frac{\mathrm{d}s^e}{\mathrm{d}t} \right)^\alpha, \tag{1}$$

where wetting dynamics is represented by $\mathrm{d}s^e/\mathrm{d}t$, and tau (i.e., τ) is assumed to be saturation-dependent as $m\,(s^e)^n$. We take the case of $M = 55.9$ (the viscosity ratio), to fit the two coefficients of m and n. Moreover, we set the power exponent, α, to 1.1, in order to be consistent with the quasi-static curve. Notice that we set the relative permeability to zero whenever $s^e - m(s^e)^n \frac{ds^e}{dt} < 0$. The fitted coefficients have the values of $m = 0.025$ and $n = -5.577$. Remarkably, the coefficients also work well when $M = 0.1$ as shown in Figure 3d. This means that a single set of coefficient values may cover a broad range of wetting dynamics. Interestingly, the proposed nonequilibrium permeability model, which is superior to the first proposed model, also predicts the critical saturation. A negative fitting value of n in Equation 1 indicates that $(s^e)^n$ helps scale wetting dynamics ($\mathrm{d}s^e/\mathrm{d}t$) to a proper range comparable to s^e.

A larger medium would be needed to cover a wide range of wetting dynamics, which will be explored in a further study. Here, instead, we simply slow down dynamics by multiplying $\mathrm{d}s^e/\mathrm{d}t$ by a value smaller than unity, to mimic different strengths of wetting dynamics. Figure 3e shows the effect of wetting dynamics on the water relative permeability for sintered glass beads, in which air is the nonwetting phase. As dynamics weakens, the water relative permeability approaches its quasi-static curve, as expected. Meanwhile, the critical water saturation reduces gradually, which is a key feature in a well-posed model for wetting relative permeability. Finally, we conduct Darcy-scale simulations of spontaneous imbibition of water into a 10 cm long medium of sintered glass beads which is initially saturated with air. We use the Van Genuchten model (van Genuchten, 1980) to fit the relationship of capillary pressure and water saturation predicted by the dynamic pore-network modeling (see Figure S3 in Supporting Information S1). This is based on the assumption that strong wetting dynamics prevails in a 10 cm long porous medium, which is justified by experimental observations of more or less constant residual saturation along the imbibition direction (Alyafei et al., 2016; Zahasky & Benson, 2019). Both the conventional wetting relative permeability model and the nonequilibrium model are tested in the simulations. The details of the two-phase Darcy modeling of spontaneous imbibition can be found in Text S2 in Supporting Information S1. Figure 3f shows the temporal water saturation profiles along the medium during spontaneous imbibition. Much sharper wetting fronts are predicted by the nonequilibrium model that are qualitatively in agreement with experimental observations (Alyafei et al., 2016; Kuijpers et al., 2017). Interestingly, we discover that the capillary pressure curve of spontaneous imbibition may accurately predict a nearly flat saturation profile behind the wetting front.

To summarize, the proposed nonequilibrium permeability model can quantitatively describe the wetting relative permeability for the early stage of spontaneous imbibition in our case studies. It also has the potential to be predictive for a wide/whole range of imbibition dynamics, which is crucial to the Darcy-scale modeling of spontaneous imbibition.

4. Conclusions

By using the pore-network modeling, we have conducted a number of case studies of cocurrent spontaneous imbibition in sintered glass beads and Estaillades. The porous medium of sintered glass beads is homogenous, while Estaillades features strong pore-scale heterogeneity. In the case studies of spontaneous imbibition of water

into the dry media, we find that pore-scale heterogeneity has significant influence on the entrapment of air, which in Estaillades is primarily due to the poor connectivity of pores, giving rise to the topological trapping. The REV size for spontaneous imbibition in Estaillades is much larger than that of a homogeneous medium. Under the assumption of uniform wettability, imbibition rates for both media can be suitably scaled with $\sqrt{cos\theta}$ (θ is the static contact angle).

Our pore-scale results show that wetting dynamics significantly deviates capillary pressure and relative permeability curves away from their quasi-static counterparts, which imposes a challenge in the Darcy-scale modeling of spontaneous imbibition. To upscale pore-scale wetting dynamics, we have proposed two relative permeability models for the wetting phase in spontaneous imbibition. We have shown that both models can predict the permeability values by the pore-network modeling. The first model is to scale the normalized saturation with respect to the critical saturation as $k_r^w = ((s^e - s_c) / (1 - s_c))^\alpha$, where $s^e = s/(1-s_r)$ is the normalized wetting saturation, s_c is the critical saturation, and α is determined by the quasi-static relative permeability curve. Although this model is brief, the critical saturation, which depends on wetting dynamics, should be predescribed. Alternatively, we developed the second model as $k_r^w = \left(s^e - m(s^e)^n \frac{\mathrm{d}s^e}{\mathrm{d}t}\right)^\alpha$, which is termed as the non-equilibrium model. The power exponent α is also determined by the quasi-static relative permeability curve. m and n are the fitting parameters. The developed nonequilibrium model can accurately predict pore-network modeling results for the early stage of spontaneous imbibition at high and low viscosity ratios. Furthermore, we have incorporated the non-equilibrium permeability model into the two-phase Darcy simulations. Much sharper wetting fronts are predicted that are qualitatively in agreement with numerous experimental findings. This indicates that the two-phase Darcy model, when supplemented by our suggested non-equilibrium permeability model, has the potential to be predictive for a broad/complete spectrum of imbibition dynamics.

Data Availability Statement

The pore-network models as well as all the data supporting this paper can be found at Qin, Chao-Zhong (2021): Data set for spontaneous imbibition in sintered glass beads and Estaillades. figshare. Data set. https://doi.org/10.6084/m9.figshare.15050472.v1). Any other material can be accessed by sending an e-mail to Chao-Zhong Qin (at chaozhong.qin@gmail.com).

Acknowledgments
Chao-Zhong Qin acknowledges the support of National Natural Science Foundation of China (No. 12072053), and the support of Human Resources and Social Security Bureau of Chongqing (No. cx2020087).

References

Aghaei, A., & Piri, M. (2015). Direct pore-to-core up-scaling of displacement processes: Dynamic pore network modeling and experimentation. *Journal of Hydrology*, *522*(2), 488–509. https://doi.org/10.1016/j.jhydrol.2015.01.004

Akbarabadi, M., & Piri, M. (2013). Relative permeability hysteresis and capillary trapping characteristics of supercritical CO_2/brine systems: An experimental study at reservoir conditions. *Advances in Water Resources*, *52*, 190–206. https://doi.org/10.1016/j.advwatres.2012.06.014

Akin, S., Schembre, J. M., Bhat, S. K., & Kovscek, A. R. (2000). Spontaneous imbibition characteristics of diatomite. *Journal of Petroleum Science and Engineering*, *25*(3–4), 149–165. https://doi.org/10.1016/S0920-4105(00)00010-3

Al-Futaisi, A., & Patzek, T. W. (2003). Impact of wettability alteration on two-phase flow characteristics of sandstones: A quasi-static description. *Water Resources Research*, *39*(2), 1–10. https://doi.org/10.1029/2002wr001366

Alyafei, N., Al-Menhali, A., & Blunt, M. J. (2016). Experimental and analytical investigation of spontaneous imbibition in water-wet carbonates. *Transport in Porous Media*, *115*(1), 189–207. https://doi.org/10.1007/s11242-016-0761-4

Alyafei, N., & Blunt, M. J. (2016). The effect of wettability on capillary trapping in carbonates. *Advances in Water Resources*, *90*, 36–50. https://doi.org/10.1016/j.advwatres.2016.02.001

Alyafei, N., & Blunt, M. J. (2018). Estimation of relative permeability and capillary pressure from mass imbibition experiments. *Advances in Water Resources*, *115*, 88–94. https://doi.org/10.1016/j.advwatres.2018.03.003

Bakhshian, S., Murakami, M., Hosseini, S. A., & Kang, Q. (2020). Scaling of imbibition front dynamics in heterogeneous porous media. *Geophysical Research Letters*, *47*(14), 1–10. https://doi.org/10.1029/2020GL087914

Bakhshian, S., Rabbani, H. S., Hosseini, S. A., & Shokri, N. (2020). New insights into complex interactions between heterogeneity and wettability influencing two-phase flow in porous media. *Geophysical Research Letters*, *47*(14), 1–10. https://doi.org/10.1029/2020GL088187

Barenblatt, G. I., Patzek, T. W., & Silin, D. B. (2003). The mathematical model of nonequilibrium effects in water-oil displacement. *SPE Journal*, *8*(4), 409–416. https://doi.org/10.2118/87329-PA

Bartels, W.-B., Rücker, M., Boone, M., Bultreys, T., Mahani, H., & Berg, S. (2019). Imaging spontaneous imbibition in full Darcy-scale samples at pore-scale resolution by fast X-ray tomography. *Water Resources Research*, *55*(8), 7072–7085. https://doi.org/10.1029/2018WR024541

Berg, S., Rücker, M., Ott, H., Georgiadis, A., van der Linde, H., Enzmann, F., et al. (2016). Connected pathway relative permeability from pore-scale imaging of imbibition. *Advances in Water Resources*, *90*, 24–35. https://doi.org/10.1016/j.advwatres.2016.01.010

Cai, J., Jin, T., Kou, J., Zou, S., Xiao, J., & Meng, Q. (2021). Lucas–Washburn equation-based modeling of capillary-driven flow in porous systems. *Langmuir*, *37*(5), 1623–1636. https://doi.org/10.1021/acs.langmuir.0c03134

Chen, S., Qin, C., & Guo, B. (2020). Fully implicit dynamic pore-network modeling of two-phase flow and phase change in porous media. *Water Resources Research*, *56*(11), 1–24. https://doi.org/10.1029/2020WR028510

Diao, Z., Li, S., Liu, W., Liu, H., & Xia, Q. (2021). Numerical study of the effect of tortuosity and mixed wettability on spontaneous imbibition in heterogeneous porous media. *Capillarity*, *4*(3), 50–62. https://doi.org/10.46690/capi.2021.03.02

Gao, Y., Qaseminejad Raeini, A., Blunt, M. J., & Bijeljic, B. (2019). Pore occupancy, relative permeability and flow intermittency measurements using X-ray micro-tomography in a complex carbonate. *Advances in Water Resources*, *129*(November), 56–69. https://doi.org/10.1016/j.advwatres.2019.04.007.2018

Gao, Y., Raeini, A. Q., Selem, A. M., Bondino, I., Blunt, M. J., & Bijeljic, B. (2020). Pore-scale imaging with measurement of relative permeability and capillary pressure on the same reservoir sandstone sample under water-wet and mixed-wet conditions. *Advances in Water Resources*, *146*(July), 103786. https://doi.org/10.1016/j.advwatres.2020.103786

Gostick, J. T. (2017). Versatile and efficient pore network extraction method using marker-based watershed segmentation. *Physical Review E*, *96*(2), 023307. https://doi.org/10.1103/PhysRevE.96.023307

Gruener, S., Sadjadi, Z., Hermes, H. E., Kityk, A. V., Knorr, K., Egelhaaf, S. U., et al. (2012). Anomalous front broadening during spontaneous imbibition in a matrix with elongated pores. *Proceedings of the National Academy of Sciences*, *109*(26), 10245–10250. https://doi.org/10.1073/pnas.1119352109

Hall, C., & Pugsley, V. (2020). Spontaneous capillary imbibition of water and nonaqueous liquids into dry quarry limestones. *Transport in Porous Media*, *135*(3), 619–631. https://doi.org/10.1007/s11242-020-01489-8

Hassanizadeh, S. M., & Gray, W. G. (1990). Mechanics and thermodynamics of multiphase flow in porous media including interphase boundaries. *Advances in Water Resources*, *13*(4), 169–186. https://doi.org/10.1016/0309-1708(90)90040-B

Haugen, Å., Fernø, M. A., Mason, G., & Morrow, N. R. (2014). Capillary pressure and relative permeability estimated from a single spontaneous imbibition test. *Journal of Petroleum Science and Engineering*, *115*, 66–77. https://doi.org/10.1016/j.petrol.2014.02.001

Joekar-Niasar, V., Hassanizadeh, S. M., & Dahle, H. K. (2010). Non-equilibrium effects in capillarity and interfacial area in two-phase flow: Dynamic pore-network modelling. *Journal of Fluid Mechanics*, *655*(April), 38–71. https://doi.org/10.1017/S0022112010000704

Krause, M. H., & Benson, S. M. (2015). Accurate determination of characteristic relative permeability curves. *Advances in Water Resources*, *83*, 376–388. https://doi.org/10.1016/j.advwatres.2015.07.009

Kuijpers, C. J., Huinink, H. P., Tomozeiu, N., Erich, S. J. F., & Adan, O. C. G. (2017). Sorption of water-glycerol mixtures in porous Al_2O_3 studied with NMR imaging. *Chemical Engineering Science*, *173*, 218–229. https://doi.org/10.1016/j.ces.2017.07.035

Lin, Q., Bijeljic, B., Foroughi, S., Berg, S., & Blunt, M. J. (2021). Pore-scale imaging of displacement patterns in an altered-wettability carbonate. *Chemical Engineering Science*, *235*, 116464. https://doi.org/10.1016/j.ces.2021.116464

Liu, Y., Cai, J., Sahimi, M., & Qin, C. (2020). A study of the role of microfractures in counter-current spontaneous imbibition by lattice Boltzmann simulation. *Transport in Porous Media*, *133*(2), 313–332. https://doi.org/10.1007/s11242-020-01425-w

Mason, G., & Morrow, N. R. (2013). Developments in spontaneous imbibition and possibilities for future work. *Journal of Petroleum Science and Engineering*, *110*, 268–293. https://doi.org/10.1016/j.petrol.2013.08.018

Mattax, C. C., & Kyte, J. R. (1962). Imbibition oil recovery from fractured, water-drive reservoir. *Society of Petroleum Engineers Journal*, *2*(02), 177–184. https://doi.org/10.2118/187-PA

Meng, Q., Liu, H., & Wang, J. (2015). Entrapment of the non-wetting phase during Co-current spontaneous imbibition. *Energy and Fuels*, *29*(2), 686–694. https://doi.org/10.1021/ef5025164

Morrow, N. R., & Mason, G. (2001). Recovery of oil by spontaneous imbibition. *Current Opinion in Colloid & Interface Science*, *6*(4), 321–337. https://doi.org/10.1016/S1359-0294(01)00100-5

Muljadi, B. P., Blunt, M. J., Raeini, A. Q., & Bijeljic, B. (2016). The impact of porous media heterogeneity on non-Darcy flow behaviour from pore-scale simulation. *Advances in Water Resources*, *95*, 329–340. https://doi.org/10.1016/j.advwatres.2015.05.019

Patzek, T. W. (2001). Verification of a complete pore network simulator of drainage and imbibition. *SPE Journal*, *6*(02), 144–156. https://doi.org/10.2118/71310-PA

Peng, S., & Xiao, X. (2017). Investigation of multiphase fluid imbibition in shale through synchrotron-based dynamic micro-CT imaging. *Journal of Geophysical Research: Solid Earth*, *122*(6), 4475–4491. https://doi.org/10.1002/2017JB014253

Qin, C., van Brummelen, H., Hefny, M., & Zhao, J. (2021). Image-based modeling of spontaneous imbibition in porous media by a dynamic pore network model. *Advances in Water Resources*, *152*(January), 103932. https://doi.org/10.1016/j.advwatres.2021.103932

Qin, C.-Z. (2021). *Dataset for spontaneous imbibition in sintered glass beads and Estaillades*. figshare dataset. https://doi.org/10.6084/m9.figshare.15050472.v1

Qin, C.-Z., & van Brummelen, H. (2019). A dynamic pore-network model for spontaneous imbibition in porous media. *Advances in Water Resources*, *133*, 103420. https://doi.org/10.1016/j.advwatres.2019.103420

Raeini, A. Q., Bijeljic, B., & Blunt, M. J. (2017). Generalized network modeling: Network extraction as a coarse-scale discretization of the void space of porous media. *Physical Review E*, *96*(1), 1–17. https://doi.org/10.1103/PhysRevE.96.013312

Rath, D., Sathishkumar, N., & Toley, B. J. (2018). Experimental measurement of parameters governing flow rates and partial saturation in paper-based microfluidic devices. *Langmuir*, *34*(30), 8758–8766. https://doi.org/10.1021/acs.langmuir.8b01345

Rokhforouz, M. R., & Akhlaghi Amiri, H. A. (2018). Pore-level influence of micro-fracture parameters on visco-capillary behavior of two-phase displacements in porous media. *Advances in Water Resources*, *113*, 260–271. https://doi.org/10.1016/j.advwatres.2018.01.030

Ruprecht, C., Pini, R., Falta, R., Benson, S., & Murdoch, L. (2014). Hysteretic trapping and relative permeability of CO_2 in sandstone at reservoir conditions. *International Journal of Greenhouse Gas Control*, *27*, 15–27. https://doi.org/10.1016/j.ijggc.2014.05.003

Sadjadi, Z., & Rieger, H. (2013). Scaling theory for spontaneous imbibition in random networks of elongated pores. *Physical Review Letters*, *110*(14), 144502. https://doi.org/10.1103/PhysRevLett.110.144502

Scanziani, A., Singh, K., Menke, H., Bijeljic, B., & Blunt, M. J. (2020). Dynamics of enhanced gas trapping applied to CO_2 storage in the presence of oil using synchrotron X-ray micro tomography. *Applied Energy*, *259*(July), 114136. https://doi.org/10.1016/j.apenergy.2019.114136

Schmid, K. S., Alyafei, N., Geiger, S., & Blunt, M. J. (2016). Analytical solutions for spontaneous imbibition: Fractional-flow theory and experimental analysis. *SPE Journal*, *21*(06), 2308–2316. https://doi.org/10.2118/184393-pa

Schmid, K. S., & Geiger, S. (2012). Universal scaling of spontaneous imbibition for water-wet systems. *Water Resources Research*, *48*(3). https://doi.org/10.1029/2011WR011566

Singh, K., & Niven, R. K. (2014). Non-aqueous phase liquid spills in freezing and thawing soils: Critical analysis of pore-scale processes. *Critical Reviews in Environmental Science and Technology*, *43*(6), 551–597. https://doi.org/10.1080/10643389.2011.604264

Soriano, J., Mercier, A., Planet, R., Hernández-Machado, A., Rodríguez, M. A., & Ortín, J. (2005). Anomalous roughening of viscous fluid fronts in spontaneous imbibition. *Physical Review Letters*, *95*(10), 1–4. https://doi.org/10.1103/PhysRevLett.95.104501

Standnes, D. C. (2010). Scaling spontaneous imbibition of water data accounting for fluid viscosities. *Journal of Petroleum Science and Engineering*, *73*(3–4), 214–219. https://doi.org/10.1016/j.petrol.2010.07.001

Standnes, D. C., & Andersen, P. Ø. (2017). Analysis of the impact of fluid viscosities on the rate of countercurrent spontaneous imbibition. *Energy and Fuels*, *31*(7), 6928–6940. https://doi.org/10.1021/acs.energyfuels.7b00863

Suo, S., Liu, M., & Gan, Y. (2019). Modelling imbibition processes in heterogeneous porous media. *Transport in Porous Media*, *126*(3), 615–631. https://doi.org/10.1007/s11242-018-1146-7

van Genuchten, M. T. (1980). A closed-form equation for predicting the hydraulic conductivity of unsaturated soils. *Soil Science Society of America Journal*, *44*(5), 892–898. https://doi.org/10.2136/sssaj1980.03615995004400050002x

Washburn, E. W. (1921). The dynamics of capillary flow. *Physical Review*, *17*(3), 273–283. https://doi.org/10.1103/PhysRev.17.273

Wijshoff, H. (2018). Drop dynamics in the inkjet printing process. *Current Opinion in Colloid & Interface Science*, *36*, 20–27. https://doi.org/10.1016/j.cocis.2017.11.004

Zahasky, C., & Benson, S. M. (2019). Spatial and temporal quantification of spontaneous imbibition. *Geophysical Research Letters*, *46*(21), 11972–11982. https://doi.org/10.1029/2019GL084532

Zarandi, M. A. F., & Pillai, K. M. (2018). Spontaneous imbibition of liquid in glass fiber wicks, Part II: Validation of a diffuse-front model. *AIChE Journal*, *64*(1), 306–315. https://doi.org/10.1002/aic.15856

Zhao, J., Qin, F., Derome, D., & Carmeliet, J. (2020). Simulation of quasi-static drainage displacement in porous media on pore-scale: Coupling lattice Boltzmann method and pore network model. *Journal of Hydrology*, *588*(May), 125080. https://doi.org/10.1016/j.jhydrol.2020.125080

Zheng, J., Lei, W., Ju, Y., & Wang, M. (2021). Investigation of spontaneous imbibition behavior in a 3D pore space under reservoir condition by lattice Boltzmann method. *Journal of Geophysical Research: Solid Earth*, *126*(6), 1–15. https://doi.org/10.1029/2021JB021987

Zhuang, L., Hassanizadeh, S. M., Qin, C.-Z., & de Waal, A. (2017). Experimental investigation of hysteretic dynamic capillarity effect in unsaturated flow. *Water Resources Research*, *53*(11), 9078–9088. https://doi.org/10.1002/2017WR020895

References From the Supporting Information

Hefny, M., Qin, C., Saar, M. O., & Ebigbo, A. (2020). Synchrotron-based pore-network modeling of two-phase flow in Nubian Sandstone and implications for capillary trapping of carbon dioxide. *International Journal of Greenhouse Gas Control*, *103*(April), 103164. https://doi.org/10.1016/j.ijggc.2020.103164

Sinha, P. K., & Wang, C.-Y. (2007). Pore-network modeling of liquid water transport in gas diffusion layer of a polymer electrolyte fuel cell. *Electrochimica Acta*, *52*(28), 7936–7945. https://doi.org/10.1016/j.electacta.2007.06.061

Thompson, K. E. (2002). Pore-scale modeling of fluid transport in disordered fibrous materials. *AIChE Journal*, *48*(7), 1369–1389. https://doi.org/10.1002/aic.690480703

Valvatne, P. H., & Blunt, M. J. (2004). Predictive pore-scale modeling of two-phase flow in mixed wet media. *Water Resources Research*, *40*(7), 1–21. https://doi.org/10.1029/2003WR002627